

Longitudinal double-spin asymmetry for inclusive jet production in $\vec{p} + \vec{p}$ collisions at $\sqrt{s}=200$ GeV

B.I. Abelev,⁹ M.M. Aggarwal,³¹ Z. Ahammed,⁴⁶ B.D. Anderson,²⁰ D. Arkhipkin,¹³ G.S. Averichev,¹²
 Y. Bai,²⁹ J. Balewski,¹⁷ O. Barannikova,⁹ L.S. Barnby,² J. Baudot,¹⁸ S. Baumgart,⁵¹ V.V. Belaga,¹²
 A. Bellingeri-Laurikainen,⁴¹ R. Bellwied,⁴⁹ F. Benedosso,²⁹ R.R. Betts,⁹ S. Bhardwaj,³⁶ A. Bhasin,¹⁹ A.K. Bhati,³¹
 H. Bichsel,⁴⁸ J. Bielcik,⁵¹ J. Bielcikova,⁵¹ L.C. Bland,³ S-L. Blyth,²³ M. Bombara,² B.E. Bonner,³⁷
 M. Botje,²⁹ J. Bouchet,⁴¹ A.V. Brandin,²⁷ T.P. Burton,² M. Bystersky,¹¹ X.Z. Cai,⁴⁰ H. Caines,⁵¹
 M. Calderón de la Barca Sánchez,⁶ J. Callner,⁹ O. Catu,⁵¹ D. Cebra,⁶ M.C. Cervantes,⁴² Z. Chajecki,³⁰
 P. Chaloupka,¹¹ S. Chattopadhyay,⁴⁶ H.F. Chen,³⁹ J.H. Chen,⁴⁰ J.Y. Chen,⁵⁰ J. Cheng,⁴⁴ M. Cherney,¹⁰
 A. Chikanian,⁵¹ W. Christie,³ S.U. Chung,³ R.F. Clarke,⁴² M.J.M. Coddington,⁴² J.P. Coffin,¹⁸ T.M. Cormier,⁴⁹
 M.R. Cosentino,³⁸ J.G. Cramer,⁴⁸ H.J. Crawford,⁵ D. Das,⁴⁶ S. Dash,¹⁵ M. Daugherty,⁴³ M.M. de Moura,³⁸
 T.G. Dedovich,¹² M. DePhillips,³ A.A. Derevschikov,³³ L. Didenko,³ T. Dietel,¹⁴ P. Djawotho,¹⁷ S.M. Dogra,¹⁹
 X. Dong,²³ J.L. Drachenberg,⁴² J.E. Draper,⁶ F. Du,⁵¹ V.B. Dunin,¹² J.C. Dunlop,³ M.R. Dutta Mazumdar,⁴⁶
 W.R. Edwards,²³ L.G. Efimov,¹² E. Elhalhuli,² V. Emelianov,²⁷ J. Engelage,⁵ G. Eppley,³⁷ B. Erasmus,⁴¹
 M. Estienne,¹⁸ P. Fachini,³ R. Fatemi,²¹ J. Fedorisin,¹² A. Feng,⁵⁰ P. Filip,¹³ E. Finch,⁵¹ V. Fine,³ Y. Fisyak,³
 J. Fu,⁵⁰ C.A. Gagliardi,⁴² L. Gaillard,² M.S. Ganti,⁴⁶ E. Garcia-Solis,⁹ V. Ghazikhanian,⁷ P. Ghosh,⁴⁶
 Y.N. Gorbunov,¹⁰ H. Gos,⁴⁷ O. Grebenyuk,²⁹ D. Grosnick,⁴⁵ B. Grube,³⁵ S.M. Guertin,⁷ K.S.F.F. Guimaraes,³⁸
 A. Gupta,¹⁹ N. Gupta,¹⁹ B. Haag,⁶ T.J. Hallman,³ A. Hamed,⁴² J.W. Harris,⁵¹ W. He,¹⁷ M. Heinz,⁵¹ T.W. Henry,⁴²
 S. Heppelmann,³² B. Hippolyte,¹⁸ A. Hirsch,³⁴ E. Hjort,²³ A.M. Hoffman,²⁴ G.W. Hoffmann,⁴³ D.J. Hofman,⁹
 R.S. Hollis,⁹ M.J. Horner,²³ H.Z. Huang,⁷ E.W. Hughes,⁴ T.J. Humanic,³⁰ G. Igo,⁷ A. Iordanova,⁹ P. Jacobs,²³
 W.W. Jacobs,¹⁷ P. Jakl,¹¹ P.G. Jones,² E.G. Judd,⁵ S. Kabana,⁴¹ K. Kang,⁴⁴ J. Kapitan,¹¹ M. Kaplan,⁸
 D. Keane,²⁰ A. Kechechyan,¹² D. Kettler,⁴⁸ V.Yu. Khodyrev,³³ J. Kiryluk,²³ A. Kisiel,³⁰ E.M. Kislov,¹²
 S.R. Klein,²³ A.G. Knospe,⁵¹ A. Kocoloski,²⁴ D.D. Koetke,⁴⁵ T. Kollegger,¹⁴ M. Kopytine,²⁰ L. Kotchenda,²⁷
 V. Kouchpil,¹¹ K.L. Kowalik,²³ P. Kravtsov,²⁷ V.I. Kravtsov,³³ K. Krueger,¹ C. Kuhn,¹⁸ A.I. Kulikov,¹²
 A. Kumar,³¹ P. Kurnadi,⁷ A.A. Kuznetsov,¹² M.A.C. Lamont,³ J.M. Landgraf,³ S. Lange,¹⁴ S. LaPointe,⁴⁹
 F. Laue,³ J. Lauret,³ A. Lebedev,³ R. Lednicky,¹³ C-H. Lee,³⁵ S. Lehocka,¹² M.J. LeVine,³ C. Li,³⁹ Q. Li,⁴⁹ Y. Li,⁴⁴
 G. Lin,⁵¹ X. Lin,⁵⁰ S.J. Lindenbaum,²⁸ M.A. Lisa,³⁰ F. Liu,⁵⁰ H. Liu,³⁹ J. Liu,³⁷ L. Liu,⁵⁰ T. Ljubicic,³
 W.J. Llope,³⁷ R.S. Longacre,³ W.A. Love,³ Y. Lu,⁵⁰ T. Ludlam,³ D. Lynn,³ G.L. Ma,⁴⁰ J.G. Ma,⁷ Y.G. Ma,⁴⁰
 D.P. Mahapatra,¹⁵ R. Majka,⁵¹ L.K. Mangotra,¹⁹ R. Manweiler,⁴⁵ S. Margetis,²⁰ C. Markert,⁴³ L. Martin,⁴¹
 H.S. Matis,²³ Yu.A. Matulenko,³³ T.S. McShane,¹⁰ A. Meschanin,³³ J. Millane,²⁴ M.L. Miller,²⁴ N.G. Minaev,³³
 S. Mioduszewski,⁴² A. Mischke,²⁹ J. Mitchell,³⁷ B. Mohanty,⁴⁶ D.A. Morozov,³³ M.G. Munhoz,³⁸ B.K. Nandi,¹⁶
 C. Nattrass,⁵¹ T.K. Nayak,⁴⁶ J.M. Nelson,² C. Nepali,²⁰ P.K. Netrakanti,³⁴ L.V. Nogach,³³ S.B. Nurushev,³³
 G. Odyniec,²³ A. Ogawa,³ V. Okorokov,²⁷ D. Olson,²³ M. Pachr,¹¹ S.K. Pal,⁴⁶ Y. Panebratsev,¹² A.I. Pavlinov,⁴⁹
 T. Pawlak,⁴⁷ T. Peitzmann,²⁹ V. Perevoztchikov,³ C. Perkins,⁵ W. Peryt,⁴⁷ S.C. Phatak,¹⁵ M. Planinic,⁵²
 J. Pluta,⁴⁷ N. Poljak,⁵² N. Porile,³⁴ A.M. Poskanzer,²³ M. Potekhin,³ E. Potrebenikova,¹² B.V.K.S. Potukuchi,¹⁹
 D. Prindle,⁴⁸ C. Pruneau,⁴⁹ N.K. Pruthi,³¹ J. Putschke,²³ I.A. Qattan,¹⁷ R. Raniwala,³⁶ S. Raniwala,³⁶ R.L. Ray,⁴³
 D. Relyea,⁴ A. Ridiger,²⁷ H.G. Ritter,²³ J.B. Roberts,³⁷ O.V. Rogachevskiy,¹² J.L. Romero,⁶ A. Rose,²³
 C. Roy,⁴¹ L. Ruan,³ M.J. Russcher,²⁹ R. Sahoo,¹⁵ I. Sakrejda,²³ T. Sakuma,²⁴ S. Salur,⁵¹ J. Sandweiss,⁵¹
 M. Sarsour,⁴² P.S. Sazhin,¹² J. Schambach,⁴³ R.P. Scharenberg,³⁴ N. Schmitz,²⁵ J. Seger,¹⁰ I. Selyuzhenkov,⁴⁹
 P. Seyboth,²⁵ A. Shabetai,¹⁸ E. Shahaliev,¹² M. Shao,³⁹ M. Sharma,³¹ W.Q. Shen,⁴⁰ S.S. Shimanskiy,¹²
 E.P. Sichtermann,²³ F. Simon,²⁴ R.N. Singaraju,⁴⁶ M.J. Skoby,³⁴ N. Smirnov,⁵¹ R. Snellings,²⁹ P. Sorensen,³
 J. Sowinski,¹⁷ J. Speltz,¹⁸ H.M. Spinka,¹ B. Srivastava,³⁴ A. Stadnik,¹² T.D.S. Stanislaus,⁴⁵ D. Staszak,⁷
 R. Stock,¹⁴ M. Strikhanov,²⁷ B. Stringfellow,³⁴ A.A.P. Suaide,³⁸ M.C. Suarez,⁹ N.L. Subba,²⁰ M. Sumner,¹¹
 X.M. Sun,²³ Z. Sun,²² B. Surrow,²⁴ T.J.M. Symons,²³ A. Szanto de Toledo,³⁸ J. Takahashi,³⁸ A.H. Tang,³
 T. Tarnowsky,³⁴ J.H. Thomas,²³ A.R. Timmins,² S. Timoshenko,²⁷ M. Tokarev,¹² T.A. Trainor,⁴⁸ V.N. Tram,²³
 S. Trentalange,⁷ R.E. Tribble,⁴² O.D. Tsai,⁷ J. Ulery,³⁴ T. Ullrich,³ D.G. Underwood,¹ G. Van Buren,³ N. van der
 Kolk,²⁹ M. van Leeuwen,²³ A.M. Vander Molen,²⁶ R. Varma,¹⁶ I.M. Vasilevski,¹³ A.N. Vasiliev,³³ R. Vernet,¹⁸
 S.E. Vigdor,¹⁷ Y.P. Viyogi,¹⁵ S. Vokal,¹² S.A. Voloshin,⁴⁹ M. Wada,¹⁰ W.T. Waggoner,¹⁰ F. Wang,³⁴ G. Wang,⁷
 J.S. Wang,²² X.L. Wang,³⁹ Y. Wang,⁴⁴ J.C. Webb,⁴⁵ G.D. Westfall,²⁶ C. Whitten Jr.,⁷ H. Wieman,²³
 S.W. Wissink,¹⁷ R. Witt,⁵¹ J. Wu,³⁹ Y. Wu,⁵⁰ N. Xu,²³ Q.H. Xu,²³ Z. Xu,³ P. Yepes,³⁷ I-K. Yoo,³⁵

Q. Yue,⁴⁴ V.I. Yurevich,¹² M. Zawisza,⁴⁷ W. Zhan,²² H. Zhang,³ W.M. Zhang,²⁰ Y. Zhang,³⁹ Z.P. Zhang,³⁹
 Y. Zhao,³⁹ C. Zhong,⁴⁰ J. Zhou,³⁷ R. Zoulkarneev,¹³ Y. Zoulkarneeva,¹³ A.N. Zubarev,¹² and J.X. Zuo⁴⁰

(STAR Collaboration)

- ¹Argonne National Laboratory, Argonne, Illinois 60439
²University of Birmingham, Birmingham, United Kingdom
³Brookhaven National Laboratory, Upton, New York 11973
⁴California Institute of Technology, Pasadena, California 91125
⁵University of California, Berkeley, California 94720
⁶University of California, Davis, California 95616
⁷University of California, Los Angeles, California 90095
⁸Carnegie Mellon University, Pittsburgh, Pennsylvania 15213
⁹University of Illinois at Chicago, Chicago, Illinois 60607
¹⁰Creighton University, Omaha, Nebraska 68178
¹¹Nuclear Physics Institute AS CR, 250 68 Řež/Prague, Czech Republic
¹²Laboratory for High Energy (JINR), Dubna, Russia
¹³Particle Physics Laboratory (JINR), Dubna, Russia
¹⁴University of Frankfurt, Frankfurt, Germany
¹⁵Institute of Physics, Bhubaneswar 751005, India
¹⁶Indian Institute of Technology, Mumbai, India
¹⁷Indiana University, Bloomington, Indiana 47408
¹⁸Institut de Recherches Subatomiques, Strasbourg, France
¹⁹University of Jammu, Jammu 180001, India
²⁰Kent State University, Kent, Ohio 44242
²¹University of Kentucky, Lexington, Kentucky, 40506-0055
²²Institute of Modern Physics, Lanzhou, China
²³Lawrence Berkeley National Laboratory, Berkeley, California 94720
²⁴Massachusetts Institute of Technology, Cambridge, MA 02139-4307
²⁵Max-Planck-Institut für Physik, Munich, Germany
²⁶Michigan State University, East Lansing, Michigan 48824
²⁷Moscow Engineering Physics Institute, Moscow Russia
²⁸City College of New York, New York City, New York 10031
²⁹NIKHEF and Utrecht University, Amsterdam, The Netherlands
³⁰Ohio State University, Columbus, Ohio 43210
³¹Panjab University, Chandigarh 160014, India
³²Pennsylvania State University, University Park, Pennsylvania 16802
³³Institute of High Energy Physics, Protvino, Russia
³⁴Purdue University, West Lafayette, Indiana 47907
³⁵Pusan National University, Pusan, Republic of Korea
³⁶University of Rajasthan, Jaipur 302004, India
³⁷Rice University, Houston, Texas 77251
³⁸Universidade de Sao Paulo, Sao Paulo, Brazil
³⁹University of Science & Technology of China, Hefei 230026, China
⁴⁰Shanghai Institute of Applied Physics, Shanghai 201800, China
⁴¹SUBATECH, Nantes, France
⁴²Texas A&M University, College Station, Texas 77843
⁴³University of Texas, Austin, Texas 78712
⁴⁴Tsinghua University, Beijing 100084, China
⁴⁵Valparaiso University, Valparaiso, Indiana 46383
⁴⁶Variable Energy Cyclotron Centre, Kolkata 700064, India
⁴⁷Warsaw University of Technology, Warsaw, Poland
⁴⁸University of Washington, Seattle, Washington 98195
⁴⁹Wayne State University, Detroit, Michigan 48201
⁵⁰Institute of Particle Physics, CCNU (HZNU), Wuhan 430079, China
⁵¹Yale University, New Haven, Connecticut 06520
⁵²University of Zagreb, Zagreb, HR-10002, Croatia

(Dated: October 24, 2018)

We report a new STAR measurement of the longitudinal double-spin asymmetry A_{LL} for inclusive jet production at mid-rapidity in polarized $p + p$ collisions at a center-of-mass energy of $\sqrt{s} = 200$ GeV. The data, which cover jet transverse momenta $5 < p_T < 30$ GeV/c, are substantially more precise than previous measurements. They provide significant new constraints on the gluon spin contribution to the nucleon spin through the comparison to predictions derived from one global fit of polarized deep-inelastic scattering measurements.

PACS numbers: 21.10, 14.20.Dh, 13.87Ce, 13.88.+e, 14.70.Dj, 13.85.Hd, 12.38.Qk

The gluon spin contribution to the nucleon spin, ΔG , has been the focus of experimental and theoretical efforts since polarized deep-inelastic scattering (DIS) experiments found that the quark contribution to the nucleon spin is small [1]. Insight into ΔG has been obtained from next-to-leading-order perturbative quantum chromodynamics (NLO pQCD) analyses of the scale dependence of the inclusive spin structure function [2, 3, 4, 5, 6, 7] and from measurements of hadroproduction of pions and photons [8]. Recent semi-inclusive DIS measurements [9] and hadroproduction measurements of jets and pions have been made [10, 11], with the latter now being incorporated in NLO pQCD fits [12]. Despite recent progress, significant uncertainty remains regarding the magnitude and sign of ΔG [13]. The inclusive measurements presented here span more than an order of magnitude in partonic momentum fraction (x) and are expected to sample a sizable piece of the total integral $\Delta G = \int_0^1 \Delta g(x) dx$. Comparisons with predictions derived from one global fit [14] to deep-inelastic scattering measurements demonstrate the substantial new constraints these results place on ΔG .

In this paper, we report a new measurement of the longitudinal double-spin asymmetry A_{LL} for mid-rapidity inclusive jet production in polarized $p + p$ collisions at $\sqrt{s} = 200$ GeV center-of-mass energy,

$$A_{LL} = \frac{\sigma^{++} - \sigma^{+-}}{\sigma^{++} + \sigma^{+-}}, \quad (1)$$

where $\sigma^{++}(\sigma^{+-})$ is the differential cross section when the beam protons have equal (opposite) helicities. We have previously measured the helicity-averaged cross section [10] for transverse momenta (p_T) up to ~ 50 GeV/c and it is well described by NLO pQCD evaluations. Inclusive jet production in the kinematic regime studied here is dominated by gluon-gluon (gg) and quark-gluon (qg) scattering. Therefore, A_{LL} provides direct sensitivity to gluon polarization [14] and the cross-section result motivates the use of NLO pQCD to interpret our measurements.

The data presented here are extracted from an integrated luminosity of 2 pb^{-1} recorded in the year 2005 with the STAR detector [15] at RHIC. The polarization was measured independently for each of the two counter-rotating proton beams and for each fill using Coulomb-Nuclear Interference (CNI) proton-Carbon polarimeters [16], which were calibrated via a polarized atomic hydrogen gas-jet target [17]. Averaged over RHIC fills, the luminosity weighted polarizations for the two beams were $52 \pm 3\%$ and $48 \pm 3\%$. The proton helicities were alternated between successive bunches in one beam and between bunch pairs in the other beam. Additionally, the helicity configurations of the colliding beam

bunches were changed between beam fills to minimize systematic uncertainties in the A_{LL} measurement. Segmented Beam-Beam Counters (BBC) [18] located up and downstream of the STAR interaction region (IR) measured the helicity dependent relative luminosities, identified minimum bias (MB) collisions, and served as local polarimeters.

The STAR subsystems used to measure jets are the Time Projection Chamber (TPC) and the Barrel Electromagnetic Calorimeter (BEMC) [15]. The TPC provides tracking for charged particles in the 0.5 T solenoidal magnetic field for pseudo-rapidities $-1.3 \lesssim \eta \lesssim 1.3$ and 2π in the azimuthal angle ϕ . In 2005 the BEMC, covering a fiducial area of $\phi = 2\pi$ and $0 < \eta < 1$, provided triggering and detection of photons and electrons.

Events were recorded if they satisfied both the MB condition, defined as a coincidence between east and west BBCs, and either a jet patch (JP) or high tower (HT) trigger. The HT condition required the energy of a single calorimeter tower to be at least 2.6 (HT1) or 3.6 (HT2) GeV. The JP trigger fired if the sum of a $\Delta\eta \times \Delta\phi = 1 \times 1$ patch of towers, the typical size of a jet, exceeded 4.5 (JP1) or 6.5 (JP2) GeV. Approximately half of the 2.38×10^6 jets extracted from the 12×10^6 event set originated from the JP2 trigger sample.

Jets were reconstructed using a mid-point cone algorithm [19] with the same parameters as described in Ref. [10]. The algorithm clusters TPC charged track momenta and BEMC tower energies within a cone radius of $R = \sqrt{\Delta\phi^2 + \Delta\eta^2} = 0.4$. Jets were required to have $p_T > 5$ GeV/c and point between $\eta = 0.2 - 0.8$ in order to minimize the effects of the BEMC acceptance on the jet energy scale. BBC timing information was used to select events with reconstructed vertex positions within ~ 60 cm of the center of the detector, ensuring uniform tracking efficiency and matching the conditions used in determining the relative luminosity measurements. Beam background from upstream sources observed as neutral energy deposits in the BEMC were minimized by requiring the neutral energy fraction of the jet energy (NEF) to be less than 0.8. A minimum NEF of 0.1 was also imposed in order to reduce pile-up effects. Finally, only jets which contained a trigger tower or pointed to a triggered jet patch were considered for analysis.

Figure 1 compares the NEF spectra for MB, HT, and JP triggered jets from data and simulations. Monte Carlo events were generated using PYTHIA 6.205 [20] with parameters adjusted to CDF 'Tune A' settings [21] and processed through the STAR detector response package based on GEANT 3 [22]. The shapes of the data distributions are sufficiently reproduced by the simulations for the purpose of estimating systematic errors. In contrast to the calorimeter triggers, the mean and shape of the

MB distribution is relatively stable as a function of jet p_T . The HT jets, and to a lesser extent the JP jets, show a strong bias towards higher NEF at low p_T which diminishes for higher jet p_T . The enhancement of jets near $\text{NEF} \approx 1$ in the data compared to simulation is consistent with contributions from beam background, as discussed above.

We present the inclusive jet A_{LL} measurement, not as a function of the measured transverse momentum (DETECTOR jet p_T), but instead corrected to reflect the jet energy scale before interaction with the STAR detector (PARTICLE jet p_T). This correction was carried out by applying the same jet reconstruction algorithm to the simulated event samples at both the PARTICLE and DETECTOR levels. PARTICLE jets are composed of stable, final-state particles which result from the fragmentation and hadronization of the scattered partons and remnant protons. DETECTOR jets consist of the reconstructed TPC tracks and BEMC tower energies in simulated events that pass the same trigger conditions that were placed on the data. As shown in Fig. 2(a) the jet yield is a rapidly falling function of jet p_T . This effect combined with the jet p_T resolution of about 25% results in a shift of the inclusive DETECTOR jet p_T distribution to larger values as shown in Fig. 2(b). For $p_T > 10$ GeV/c the reconstructed DETECTOR jet p_T is on average a factor 1.22 larger than the PARTICLE jet p_T . This shift varies only slightly with trigger and underlying partonic process (gg vs. qg vs. qq). The dominant uncertainty in the jet p_T values arises from the $\pm 4\%$ uncertainty in the jet energy scale, but we also account for the subsample dependence in the DETECTOR to PARTICLE jet conversion. The agreement between data and simulations is best at high p_T (as shown in Fig.1) where the correction, proportional to p_T , is largest. The uncertainty in the PARTICLE jet p_T slope results in a $\pm 2.5\%$ error on the p_T scale.

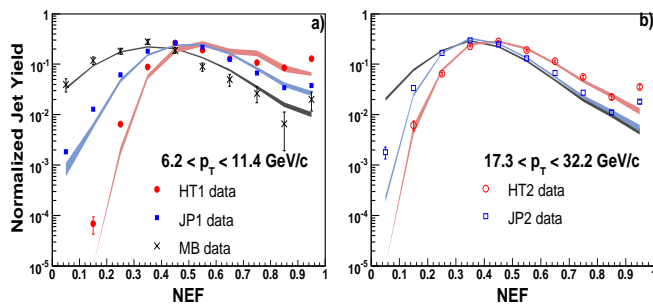


FIG. 1: Neutral energy fraction of the jet energy for MB (crosses), HT (circles), and JP (squares) data compared with STAR simulations for two jet p_T bins, (a) $6.2 < p_T < 11.4$ GeV/c and (b) $17.3 < p_T < 32.2$ GeV/c. The statistical uncertainties are represented as error bars for the data points and bands for the simulations. (Color available on-line)

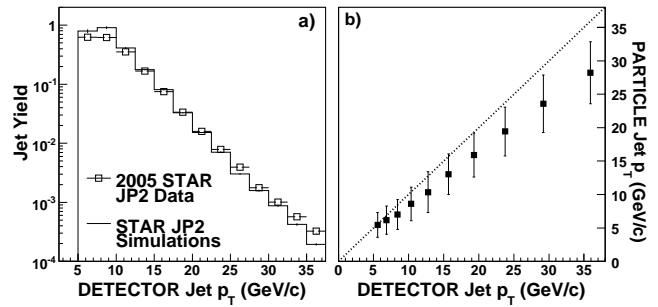


FIG. 2: (a) The raw detected jet yield in data (points) compared with the STAR Monte Carlo simulations. (b) Correlation between the reconstructed jet transverse momenta at the PARTICLE and DETECTOR levels. The points indicate the means and the vertical error bars show the r.m.s. widths of the associated PARTICLE jet distributions within the DETECTOR jet bins. The dashed line represents the condition when the PARTICLE and DETECTOR jet p_T values are equal.

The asymmetry A_{LL} was evaluated according to,

$$A_{LL} = \frac{\sum (P_1 P_2) (N^{++} - RN^{+-})}{\sum (P_1 P_2)^2 (N^{++} + RN^{+-})}, \quad (2)$$

in which $P_{1,2}$ are the measured beam polarizations, N^{++} and N^{+-} denote the inclusive jet yields for equal and opposite proton beam helicity configurations, and R is the measured relative luminosity. Each sum is over 10 to 30 minute long runs, a period much shorter than typical time variations in critical quantities such as $P_{1,2}$ and R . Typical values of R range from 0.85 to 1.2 depending on fill and bunch pattern.

Figure 3 shows the results for inclusive jet A_{LL} versus jet p_T corrected for detector response to the particle level. The vertical error bars show the statistical uncertainties. The height of the gray band on each data point indicates the total systematic uncertainty on A_{LL} while the width reflects the systematic uncertainty on jet p_T . An overall 9.4% scale error due to the uncertainty in the RHIC CNI polarimeter calibration is not included in the systematic error shown in Fig. 3. The present results are in good agreement ($\chi^2/ndf = 7.3/6$) with our previous measurements of A_{LL} [10]. The combined statistical and systematic asymmetry uncertainties are reduced by a factor of 4 and the p_T coverage is nearly doubled, extending up to 30 GeV/c.

The curves shown in Fig. 3 are NLO pQCD evaluations for A_{LL} based on different polarized parton distribution functions [14]. The curve labeled GRSV-std uses the best fit to the inclusive DIS data ($\Delta g(x, Q_0^2) = 0.24$) at the initial scale $Q_0^2 = 0.4$ GeV²/c² of the parton parametrizations in Ref. [4]. The other curves correspond to maximally positive ($\Delta g(x, Q_0^2) = g$), maximally negative ($\Delta g(x, Q_0^2) = -g$) and vanishing ($\Delta g(x, Q_0^2) = 0$) gluon polarization. The calculations were performed with factorization and renormalization scales $\mu_F = \mu_R = p_T$.

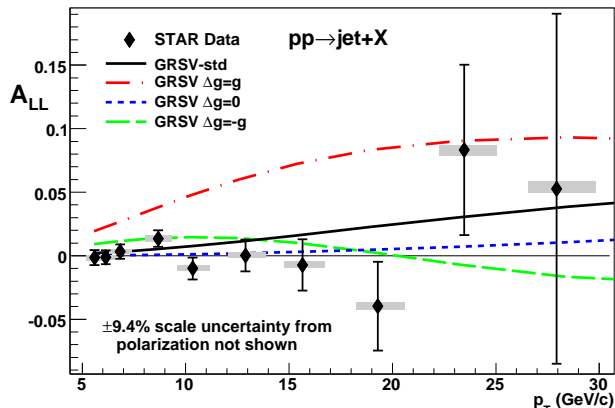


FIG. 3: Longitudinal double-spin asymmetry A_{LL} for inclusive jet production at $\sqrt{s} = 200$ GeV versus jet p_T . The points show results for PARTICLE jets with statistical error bars, while the curves show predictions for NLO parton jets from one global analysis [14]. The gray boxes indicate the systematic uncertainties on the measured A_{LL} values (vertical) and in the corrections to the measured jet p_T and the conversion between PARTICLE jet and NLO parton jet p_T (horizontal). (Color available on-line.)

The A_{LL} values for the GRSV-std and $\Delta g(x, Q_0^2) = g$ cases change by less than 20% for variations in the scale from $p_T/2$ to $2p_T$. The calculations are performed for jets composed of NLO partons which do not include effects due to hadronization and the underlying event. This difference, estimated from simulation studies, causes a $^{+4}_{-0}\%$ systematic shift in jet p_T between PARTICLE and NLO parton jets.

The leading systematic error contribution to the A_{LL} measurement arises from trigger and reconstruction effects which cause the asymmetry to differ for PARTICLE and DETECTOR jets. The shift in jet energy scale results in the smearing of the PARTICLE jet A_{LL} across the detected jet p_T bin, an effect which is largely accounted for by the correction of measured DETECTOR jet to PARTICLE jet p_T values. The calorimeter triggers, designed to select a subset of all minimum bias events, change the natural distribution of qq , qg and gg events which comprise the inclusive measurement. The consequence of this change for A_{LL} also depends on the true value of the gluon helicity distribution. Therefore the systematic error due to both triggering and reconstruction bias was estimated from the jet asymmetries calculated within the simulation framework for GRSV-std, $\Delta g(x, Q_0^2) = 0$, and $\Delta g(x, Q_0^2) = -g$ scenarios. The $\Delta g(x, Q_0^2) = g$ scenario, shown in Fig. 3, is not consistent with our data and therefore was not included in the estimates. The maximum positive and negative differences for the distributions were selected at each p_T bin. Other systematic uncertainties include effects from relative luminosities (9×10^{-4}), beam background (7×10^{-4}) and non-longitudinal beam polarization components at the STAR

IR (3×10^{-4}). Parity violating single-spin asymmetries in the data were found to be consistent with zero, < 0.2 standard deviation, as expected, given that parity violating physical processes are predicted to be negligible at the current level of statistics.

Figure 4a illustrates the gluon x range accessed in a low and high p_T data bin. Note that the sampled $\Delta g(x)$ distributions depend on the magnitude and momentum-dependence of the gluon polarization and may have very different shapes. The smooth curve represents the corresponding fraction of ΔG sampled for $x_{min} = x_{gluon}$ in the GRSV-std scenario at a scale of $Q^2 = 100 \text{ GeV}^2/c^2$ which is typical for the present data. The measurements presented here provide sensitivity to $\sim 50\%$ of ΔG .

To quantify the impact of the new data on ΔG , the measured A_{LL} values have been compared to predictions within the GRSV framework [4, 14, 23] in which the polarized parton distributions were re-fit assuming ΔG is constrained to a series of values spanning the full range $-g \leq \Delta g(x, Q_0^2) \leq g$. Figure 4b shows the confidence levels (C.L.) found from comparisons with this inclusive jet data. The correlations among the systematic uncertainties for various jet p_T have been included in the C.L. calculations.

We find that the presented data exclude fits of $\Delta G > 0.33$ at a scale of $0.4 \text{ GeV}^2/c^2$ with at least 90% C.L. and the $\Delta g(x, Q^2) = -g$ scenario is excluded at the 94% level. As discussed in Ref. [4], the GRSV-std fit to the existing DIS world data corresponded to a $\Delta G(Q_0^2 = 0.4) = 0.24$ with a range of $-0.45 < \Delta G < 0.7$ allowed with a χ^2 variation of 1. Although these conclusions are dependent on the functional form for the gluon polarization defined in the GRSV framework, the constraints placed by our data on the slice of ΔG between $x=0.02-0.2$ are significant and will exclude additional PDF's which have a $\Delta G = \int_{0.02}^{0.2} \Delta g(x) dx$ contribution larger than GRSV-std in this x region.

In summary, we report new measurements of the longitudinal double-spin asymmetry A_{LL} for inclusive jet production at mid-rapidity in polarized $p + p$ collisions at $\sqrt{s} = 200$ GeV with coverage in jet transverse momentum up to $30 \text{ GeV}/c$ and improved precision compared to previous measurements. The data have been compared to predictions of A_{LL} within the GRSV framework, a commonly used set of polarized parton distribution functions, constraining $\Delta G(Q_0^2)$ to less than 65% of the proton spin with 90% confidence. A global analysis of DIS and RHIC data is needed to realize the full impact of these results on the shape and magnitude of $\Delta g(x, Q^2)$.

The authors thank W. Vogelsang and M. Stratmann for providing calculations and discussion. We thank the RHIC Operations Group and RCF at BNL, and the NERSC Center at LBNL for their support. This work was supported in part by the Offices of NP and HEP within the U.S. DOE Office of Science; the U.S. NSF; the BMBF of Germany; CNRS/IN2P3, RA, RPL, and EMN

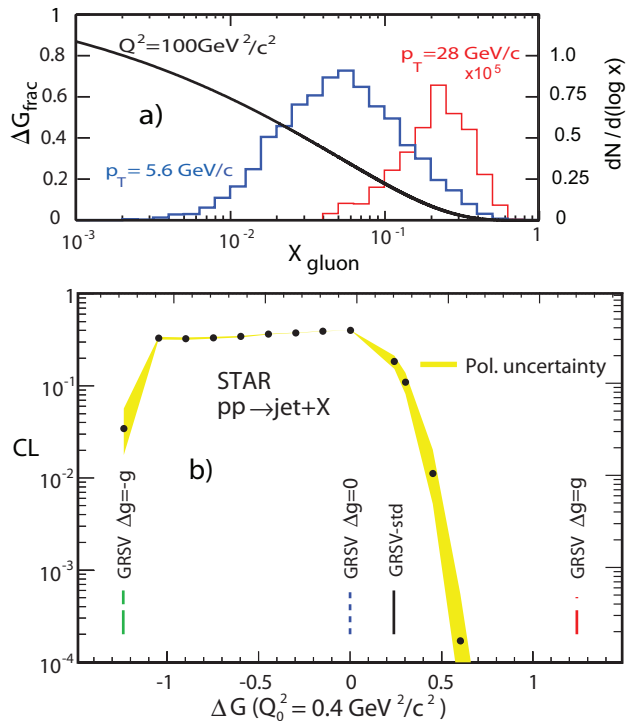


FIG. 4: (a) The solid curve represents the fraction of ΔG for GRSV-std that has $x > x_{min}$ for scale $Q^2 = 100 \text{ GeV}^2/c^2$. The histograms show the x_{gluon} sampled in the lowest and highest jet p_T bins. (b) Confidence levels for several gluon polarization distributions, characterized by their ΔG at an input scale of $0.4 \text{ GeV}^2/c^2$ [4, 14, 23] (Color available on-line).

of France; EPSRC of the United Kingdom; FAPESP of Brazil; the Russian Ministry of Education and Science; the Ministry of Education and the NNSFC of China; IRP and GA of the Czech Republic, FOM of the Netherlands, DAE, DST, and CSIR of the Government of India; Swiss NSF; the Polish State Committee for Scientific Research; SRDA of Slovakia, and the Korea Sci. & Eng. Foundation.

- E. S. Ageev *et al.*, Phys. Lett. B **633**, 25 (2006).
 [10] B. I. Abelev *et al.*, Phys. Rev. Lett. **97**, 252001 (2006).
 [11] S. S. Adler *et al.*, Phys. Rev. D **73**, 091102 (2006).
 [12] M. Hirai, S. Kumano and N. Saito, Phys. Rev. D **74**, 014015 (2006). G. A. Navarro and R. Sassot, Phys. Rev. D **74**, 011502 (2006).
 [13] E. Leader, A. V. Sidorov and D. B. Stamenov, Phys. Rev. D **75**, 074027 (2007).
 [14] B. Jäger, M. Stratmann and W. Vogelsang, Phys. Rev. D **70**, 034010 (2004).
 [15] Special Issue: RHIC and its Detectors (*and references within*) Nucl. Instrum. Meth. A **499**, 624 (2003).
 [16] O. Jinnouchi *et al.*, arXiv:nucl-ex/0412053.
 [17] H. Okada *et al.*, arXiv:hep-ex/0601001.
 [18] J. Koryluk *et al.*, hep-ex/0501072.
 [19] G. C. Blazey *et al.*, arXiv:hep-ex/0005012.
 [20] T. Sjostrand, L. Lonnblad and S. Mrenna, arXiv:hep-ph/0108264.
 [21] CDF, R. Field and R. C. Group, arXiv:hep-ph/0510198.
 [22] Geant 3.21, CERN Program Library.
 [23] M. Stratmann and W. Vogelsang, private communication (2006).

- [1] J. Ashman *et al.*, Nucl. Phys. B **328**, 1 (1989). B. W. Filippone and X. D. Ji, Adv. Nucl. Phys. **26**, 1 (2001).
 [2] B. Adeva *et al.*, Phys. Rev. D **58**, 112002 (1998).
 [3] P. L. Anthony *et al.*, Phys. Lett. B **493**, 19 (2000).
 [4] M. Glück, E. Reya, M. Stratmann and W. Vogelsang, Phys. Rev. D **63**, 094005 (2001).
 [5] D. de Florian, G. A. Navarro and R. Sassot, Phys. Rev. D **71**, 094018 (2005).
 [6] E. Leader, A. V. Sidorov and D. B. Stamenov, Phys. Rev. D **73**, 034023 (2006).
 [7] A. Airapetian *et al.*, Phys. Rev. D **75**, 012007 (2007).
 [8] D. L. Adams *et al.*, Phys. Lett. B **261**, 197 (1991).
 D. L. Adams *et al.*, Phys. Lett. B **336**, 269 (1994).
 [9] A. Airapetian *et al.*, Phys. Rev. Lett. **84**, 2584 (2000).
 B. Adeva *et al.*, Phys. Rev. D **70**, 012002 (2004).

TABLE I: A_{LL} for inclusive jet production in jet p_T bins with statistical (stat) and systematic (sys) uncertainties. Both the average measured jet p_T , $\langle p_T^M \rangle$, and the final shifted jet p_T with associated systematics are reported.

$\langle p_T^M \rangle$ (GeV/c)	$\langle p_T \rangle + \text{sys.} - \text{sys.}$ (GeV/c)	$A_{LL} \pm \text{stat} + \text{sys} - \text{sys}$ ($\times 10^{-3}$)
5.58	5.60 +0.36 -0.41	$-1.51 \pm 5.92 +2.11 -2.11$
6.84	6.14 +0.46 -0.48	$-1.16 \pm 5.44 +1.77 -1.90$
8.38	6.83 +0.53 -0.54	$3.27 \pm 5.59 +1.61 -1.86$
10.26	8.67 +0.65 -0.61	$13.51 \pm 6.53 +2.91 -2.15$
12.57	10.34 +0.83 -0.76	$-10.01 \pm 8.58 +2.60 -1.71$
15.41	12.89 +0.96 -0.83	$0.19 \pm 12.59 +2.77 -1.78$
18.90	15.65 +1.09 -0.88	$-7.30 \pm 20.21 +3.09 -2.22$
23.20	19.30 +1.31 -1.02	$-39.69 \pm 34.84 +2.99 -2.99$
28.39	23.48 +1.59 -1.19	$83.17 \pm 67.03 +4.10 -4.10$
34.81	27.94 +1.88 -1.37	$52.70 \pm 137.65 +5.74 -3.73$